Preprints (www.preprints.org) | NOT PEER-REVIEWED | Posted: 30 November 2019 doi:10.20944/preprints201911.0391.v1

Article

The Determination of Snow Albedo from Satellite Measurements Using Fast Atmospheric Correction Technique

Alexander Kokhanovsky[1], Jason E. Box[2], Baptiste Vandecrux[2], Kenneth Mankoff[2], Maxim Lamare[3], Alexander Smirnov[4], and Michael Kern[5]

[1] VITROCISET, Bratustrasse 7, D-64293 Darmstadt, Germany; a.kokhanovsky@vitrocisetbelgium.com
[2] Geological Survey of Denmark and Greenland (GEUS), Copenhagen, Denmark
[3] Météo-France, CNRS, CNRM, Centre d'Etudes de la Neige, Grenoble, France
[4] Science Systems and Applications, Inc., Lanham, Maryland, USA, and Biospheric Sciences Laboratory, NASA GSFC, Greenbelt, Maryland, USA
[5] ESTEC/ESA, Science, Applications and Climate Department (EOP-SME), Noordwijk, The Netherlands

A.Kokhanovsky, a.kokhanovsky@vitrocisetbelgium.com
J. E. Box, jeb@geus.dk
B. Vandecrux, bav@geus.dk
K. Mankoff@geus.dk
M. Lamare, maxim.lamare@meteo.fr
A. Smirnov, alexander.smirnov-1@nasa.gov
M. Kern, Michael.Kern@esa.int

* Correspondence: a.kokhanovsky@vitrocisetbelgium.com

Abstract: We present a simplified atmospheric correction algorithm for the snow/ice albedo retrieval using single view satellite measurements. The validation of the technique is performed using Ocean and Land Colour Instrument (OLCI) on board Copernicus Sentinel - 3 satellite and ground spectral or broadband albedo measurements from locations on the Greenland ice sheet and in the French Alps. Through comparison with independent ground observations, the technique is shown to perform accurately in a range of conditions from a 2100 m elevation mid-latitude location in the French Alps to a network of 15 locations across a 2390 m elevation range in seven regions across the Greenland ice sheet. Retrieved broadband albedo is accurate within 5% over a wide (0.5) broadband albedo range of the (N = 4,155) Greenland observations and with no apparent bias.

Keywords: snow characteristics; optical remote sensing; snow albedo; PROMICE; Sentinel 3, OLCI; atmospheric correction; Arctic aerosol

---

1. Introduction

There is a decreasing trend in both the extent and reflective power of the terrestrial cryosphere with important feedbacks amid global warming [1-4]. The solar light reflectance from snow and ice has a bi-directional nature. It depends on the direction of illumination and also on the observation direction which can be measured using ground, airborne, and satellite optical instruments. Climate models utilize snow spectral plane albedo, which provides total reflected solar light power for a given wavelength and a given solar incidence angle, which depends on the location and time. Satellite

 doi:10.20944/preprints201911.0391.v1

measurements, of particular importance for studies of polar environment [4], are usually performed with a fixed observation geometry. Therefore, special procedures are needed to convert satellite – measured reflectance to a planar albedo [5, 6]. The broadband plane albedo (BBA) can be derived using various parameterizations or by integration of the spectral plane albedo with account for the spectral snow irradiance at the snow surface [7]. The optical signals measured by satellite are influenced not just by light reflected from the surface but by atmospheric extinction, i.e., scattering and absorption processes. Therefore, atmospheric effects must be removed for a useful surface retrieval. Similarly, the remote sensing of the atmosphere requires removal of the surface contribution to the observed signal. Atmospheric remote sensing of the atmosphere is more readily made in cases of dark underlying surfaces, such as the ocean. In polar regions, the retrievals of atmospheric aerosol load over bright snow and ice surfaces are challenging and often hardly possible because the signal is dominated by the surface properties and not by atmospheric aerosol, which have a much smaller loading as compared to aerosols over lower latitude land surfaces covered by vegetation and bare soil.

A key task of this study is to provide an accurate determination of spectral and broadband plane albedo of snow and ice using satellite observations given the challenge of atmospheric absorption by ozone, molecular light scattering and light scattering and absorption by atmospheric aerosols. It is assumed that aerosol optical properties are known a priori, e.g., from aerosol climatology, forecasts or ground measurements for the case of polluted snow/atmosphere. In the case of clean snow and atmosphere, we do not rely on any a priori information on atmospheric aerosol loading and properties in our snow and ice albedo retrieval technique. In any case, the generally low polar aerosol loading [4] reduces the influence of the aerosol contribution to the retrieved surface albedo. Although in many cases the atmospheric contribution cannot be neglected. In the case of polluted snow, the retrievals are performed outside strong atmospheric absorption bands (e.g., O_2 and H_2O). The ozone absorption effects are fully accounted in the retrieval framework. While the algorithm is easily portable to other multi-spectral instruments observing the cryosphere from space, we present an application to data from the Ocean and Land Colour Instrument (OLCI) on board the European Union Copernicus Sentinel-3A satellite. The theoretical modelling of spectral snow reflectance is performed as in [6]. The earlier atmospheric correction used in [6], that appears in OLCI Snow Properties module incorporated in the ESA SeNtinel Application Platform (SNAP), can be biased in case of strong atmospheric pollution episodes (Arctic haze, etc.) because it neglects scattering and absorption by liquid and solid particles suspended in atmosphere. This shortcoming of the previous algorithm as presented in [6] is eliminated in this study.

2. **Materials and methods**

2.1 Theory

We perform the retrievals using separate retrieval chains for the clean snow (Case 1 clean snow) and for polluted snow (Case 2 polluted snow). Here, we use the analogy with the classification of Case 1 and Case 2 water as proposed in [8] (see also [9]). Case 1 water corresponds to relatively clean water where most of the absorption is due to phytoplankton and Case 2 water contains other impurities including mineral particles. In our application, we define Case 1 as the situation where snow properties are determined just by snow grains without significant interference from impurities or living matter (cells, algae, etc.). The clean snow Case 1 is often met in Antarctica – far from any significant aerosol sources and limited algal populations. The areal extent of the clean dry snow areas on the Greenland and Antarctica ice sheets make the Case 1 snow dominant on a global scale. Additionally, a simplified atmospheric correction is possible in this case [6].

Case 1 clean snow

Preprints (www.preprints.org) | NOT PEER-REVIEWED | Posted: 30 November 2019 doi:10.20944/preprints201911.0391.v1

The simplified atmospheric correction for Case 1 snow is described in [6] and summarized below. It is based on the fact that the pure snow spherical albedo can be accurately parameterized using the following equation:

$$r_s = \exp\left(-\sqrt{\alpha(\lambda)l}\right), \tag{1}$$

where $\alpha(\lambda)$ is the bulk ice absorption co efficient known known from laboratory experiments for a given wavelength λ and l is the effective absorption length (EAL). The snow spectral reflectance R_s is related to the snow spherical albedo, which is three dimensional integral of R_s with respect to the solar and viewing zenith angles and relative azimuthal angle (RAA)[6], via the following approximate equation [6]:

$$R_s = R_0 r_s^x, \tag{2}$$

where x is a geometrical correction coefficient depending on R_0 and on the angular function u [6] evaluated at the cosine of the solar zenith angle (SZA) μ_0 and at the cosine of the viewing zenith angle(VZA) μ:

$$x = \frac{u(\mu_0)u(\mu)}{R_0} \tag{3}$$

and we use the following approximation for the angular function [6]:

$$u(z) = \frac{3}{7}(1 + 2z). \tag{4}$$

The value of R_0 gives the non-absorbing underlying surface reflectance ($r_s = 1$). One can use OLCI measurements at 865 and 1020nm to determine both EAL and R_0 from Eqs. (1), (2) under assumption that the atmosphere does not affect the satellite signal at these channels.

The determined value of EAL makes it possible to derive the snow spherical albedo at any wavelength using Eq. (1). The plane albedo r_p is defined via the integral of the plane albedo with respect to the solar zenith angle[6]. As a matter of fact, r_p can be derived from the spherical albedo using the following simple approximation [6]:

$$r_p = r_s^{u(\mu_0)} \tag{5}$$

or with account for Eq. (1):

$$r_p = \exp\left(-u(\mu_0)\sqrt{\alpha(\lambda)l}\right) \tag{6}$$

Also one can derive the underlying snow spectral reflectance function using Eqs. (1) and (2). Therefore, the procedure for the determination of Case 1 spectral albedo from space is straightforward. It has been validated in [6]. Generally, the errors in the retrieved albedo are below 1-3% depending on the wavelength λ .

Case 2 polluted snow

The retrievals for the Case 2 snow are more complicated. In this case, the satellite measurements of snow spectral reflectance in the visible are influenced by various pollutants or living matter (cells, algae, etc.). Therefore, there is no way to estimate snow spectral reflectance/albedo in the visible using measurements in the near infrared as it is done for the Case 1 clean snow (see above). Then we use yet another approach described below.

The top-of-atmosphere reflectance for atmosphere-underlying snow system can be presented in the following way [10, 11]:

$$R_{meas} = R_{ag} + \frac{T_{ag} r_s}{1 - r_{ag} r_s}, \tag{7}$$

where R_{ag} is the atmospheric contribution to the measured signal, r_{ag} is the spherical albedo of the atmosphere, r_s is the bottom-of-atmosphere snow spherical albedo, T_{ag} is atmospheric transmittance

Preprints (www.preprints.org) | NOT PEER-REVIEWED | Posted: 30 November 2019 doi:10.20944/preprints201911.0391.v1

from the top-of-atmosphere to the underlying surface and back to the satellite position. In the case of Lambertian underlying surfaces, the underlying surface reflectance does not depend on solar and viewing observation directions and Eq. (7) is valid with $r_s = R_s$, where R_s is underlying Lambertian surface reflectance. The snow is not exactly Lambertian reflector, therefore, we replace r_s in the numerator of Eq. (7) by the snow reflectance (see Eq. (2)). Then it follows:

$$R_{meas} = R_{ag} + \frac{T_{ag}R_0 r_s^x}{1 - r_{ag}r_s}. \tag{8}$$

The reflectance of nonabsorbing snow R_0 in Eq. (8) can be calculated using simple analytical approximation as discussed in [6].

We shall use channels not influenced by water vapor and oxygen absorption effects. Although we account for the ozone absorption effects. Eq. (8) is very general and valid outside and inside molecular absorption bands. We account for the ozone absorption in a simplified way. Namely, we derive free of ozone absorption top-of-atmosphere reflectance R_c using the following equation: $R_c = \frac{R_{meas}}{T_{O3}}$, where T_{O3} is the atmospheric transmittances with account for the ozone absorption (see Appendix). Then Eq. (8) is transformed to a simplified approximation:

$$R_c = R_a + \frac{T_a R_0 r_s^x}{1 - r_a r_s}, \tag{9}$$

where the functions R_a, r_a, T_a (see Appendix) have the same meaning as R_{ag} r_{ag}, T_{ag}, respectively, except for atmosphere not influenced by gaseous absorption processes (e.g., ozone absorption). The spherical albedo of underlying snow surface can be found from Eq. (9) providing that the aerosol model is known. In this case the snow spherical albedo r_s is the only unknown parameter in Eq. (9) and can be readily calculated solving the transcendent Eq. (9) with respect to r_s . For the wavelengths, where the aerosol contribution is low and can be neglected, $R_a \sim 0$, $T_a \sim 1$, and an analytical solution of Eq. (9) is possible:

$$r_s = \left(\frac{R_c}{R_0}\right)^{1/x}, \tag{10}$$

where the analytical expression for R_0 is given in [6]. The functions R_a, T, and r_a depend on aerosol and molecular scattering parameters and can be stored in look-up-tables for various aerosol models. Because, aerosol load is weak in Arctic and Antarctica, various approximations for the functions mentioned above can be used. In particular, we calculate these functions in the framework of approximations described in Appendix. We solve the transcendent Eq. (9) with respect to r_s for all OLCI wavelengths free of water vapor and oxygen absorption in the Case 2 snow.

The broadband albedo (BBA), either plane or spherical, is calculated from the spectral plane or spherical albedo using the integration between the wavelengths λ_a and λ_b as shown below [7]:

$$\bar{r}_{p,s}(\lambda_1, \lambda_2) = \frac{\int_{\lambda_a}^{\lambda_b} r_{p,s}(\lambda)F(\lambda)d\lambda}{\int_{\lambda_a}^{\lambda_b} F(\lambda)d\lambda}. \tag{11}$$

where $F(\lambda)$ is the incident solar flux at the snow surface, $r_{p,s}(\lambda)$ is plane (p) or spherical (s) albedo depending on whether plane or spherical BBA $\bar{r}_{p,s}(\lambda_a, \lambda_b)$ is to be calculated. The indices a and b signify the wavelengths λ used. We assume that the incident solar flux can be approximated by the following analytical function:

$$F(\lambda) = f_0 + f_1 \exp(-\psi\lambda) + f_2 \exp(-\gamma\lambda), \tag{12}$$

where we ignored rapid oscillations of $F(\lambda)$, which are due to gaseous absorbers. This is possible because $r_{p,s}(\lambda)$ is a continuous function, which acts as a filter of high frequencies. The coefficients in Eq. (12) are derived from the fit of $F(\lambda)$ calculated using the Santa Barbara DISORT Radiave Transfer (SBDART) code [12] to Eq. (12) in the spectral range 0.3-2.4 μm. They are given in Table 1. The calculations of $F(\lambda)$ have been performed at the parameters listed in Table 2 for the rural aerosol

Preprints (www.preprints.org) | NOT PEER-REVIEWED | Posted: 30 November 2019 doi:10.20944/preprints201911.0391.v1

model [13]. The spectral snow albedo needed as input for SBDART has been calculated assuming clean snow with the effective diameter of spherical ice grains equal to 0.25mm. Generally, the results are only weakly sensitive to the variation of the function $F(\lambda)$[7]. We, therefore, assume solar flux independent from the location of the retrieval and from solar zenith angles.

Table 1. The coefficients of approximation given by Eq. (12)

f_0	f_1	f_2	ψ, 1/microns	γ, 1/microns
3.238e+1	-1.6014033e+5	7.95953e+3	1.778e+3	2.489e+1

Table 2. The parameters of calculations performed using SBDART

Parameter	Value
Water vapor column	2.085g/m^2
Total ozone column	350 DU
Tropospheric ozone	34.6DU
Aerosol optical thickness at 550nm	0.1
Altitude	825m
Solar zenith angle	60 degrees

For the Case 1 snow, the broadband albedo is calculated numerically using Eqs. (11), (1), (5), (12) in the spectral range 0.3-2.4 micrometers. Also other limits of integration can be used (say, to derive visible or near-infrared BBA).

For the Case 2 snow, the spherical albedo is known only for selected OLCI channels as derived from Eq. (9). Therefore, we use interpolation to get the spherical albedo between the measurement points needed for the evaluation of integral (11). For the spectral range below 865 nm, we use:

$$r_s = c\lambda^2 + b\lambda + a. \tag{13}$$

While for wavelength larger than 865 nm we use:

$$r_s = \sigma \exp(-\epsilon\lambda). \tag{14}$$

The coefficients *(a,b,c)* are found separately for the intervals 400-709nm and 709-865nm using the following wavelength triplets: (400, 560, 709nm) and (709, 753, and 865nm), respectively.

The coefficients (ϵ, σ) are derived from OLCI measurements at 865 and 1020nm at the value of R_{meas}*(1020nm)* < 0.5. Otherwise, Eq. (1) (and not Eq. (14)) is used at $\lambda > 865nm$ with the EAL derived from the value of spherical albedo at 1020nm.

Integral (11) for the spherical broadband albedo with account for Eqs. (12) - (14) can be evaluated analytically. The answer is:

$$\bar{r}_s(\lambda_a, \lambda_b) = \bar{r}_{s1}(\lambda_a, \lambda_1) + \bar{r}_{s2}(\lambda_1, \lambda_2) + \bar{r}_{sd}(\lambda_2, \lambda_b), \tag{15}$$

where

$$\bar{r}_{sj}(\lambda_a, \lambda_b) = a_j + (b_j K(\lambda_a, \lambda_b) + c_j L(\lambda_a, \lambda_b))/J(\lambda_a, \lambda_b),$$

$$\bar{r}_{sd}(\lambda_a, \lambda_b) = M(\lambda_a, \lambda_b)/J(\lambda_a, \lambda_b),$$

$$J(\lambda_a, \lambda_b) = f_0 j_0 + f_1 i_1(\psi) + f_2 i_1(\gamma),$$

$$K(\lambda_a, \lambda_b) = f_0 k_0 + f_1 i_2(\psi) + f_2 i_2(\gamma), \tag{16}$$

$$L(\lambda_a, \lambda_b) = f_0 l_0 + f_1 i_3(\psi) + f_2 i_3(\gamma),$$

Preprints (www.preprints.org) | NOT PEER-REVIEWED | Posted: 30 November 2019 doi:10.20944/preprints201911.0391.v1

$$M(\lambda_a, \lambda_b) = \sigma(f_0 i_0(\epsilon) + f_1 i_0(\epsilon + \psi) + f_2 i_0(\epsilon + \gamma)).$$

Here the coefficients a_j, b_j, c_j are the same as presented in Eq. (13) with *j=1* for the first spectral interval (0.3-0.709 microns) and *j=2* for the second spectral interval (0.709-0.865 microns), $\lambda_a = 0.3\mu m, \lambda_1 = 0.709\ \mu m, \lambda_2 = 0.865\mu m, \lambda_b = 2.4\ \mu m$, $J(\lambda_a, \lambda_b)$ is the integral given in the dominator in Eq. (11) (evaluated analytically with account for Eq. (12)) and

$$j_0 = \lambda_b - \lambda_a, k_0 = (\lambda_b^2 - \lambda_a^2)/2, l_0 = (\lambda_b^3 - \lambda_a^3)/3,$$

$$i_1(v) = (\exp(-v\lambda_a) - \exp(-v\lambda_b))/v,$$

$$i_2(v) = (\frac{1}{v^2} + \frac{\lambda_a}{v})\exp(-x\lambda_a) - (\frac{1}{v^2} + \frac{\lambda_2}{v})\exp(-v\lambda_b), \quad (17)$$

$$i_3(v) = (\frac{2}{v^3} + \frac{2\lambda_a}{v^2} + \frac{\lambda_a^2}{v})\exp(-v\lambda_a) - (\frac{2}{v^3} + \frac{2\lambda_b}{v^2} + \frac{\lambda_b^2}{v})\exp(-v\lambda_b).$$

At the of *R(1020nm)* equal or above 0.5, the analytical expression for the BBA can not be derived (because one accounts for Eq. (1) (not Eq. (13)) in Eq. (11)). Then the numerical integration procedure is followed.

The broadband plane albedo is calculated in a similar way as a broadband spherical albedo using Eq.(5) for the transformation of spherical to plane albedo.

This concludes the description of this new fast radiative transfer Snow and ICE surface albedo retrieval (SICE) that accounts for atmospheric scattering and absorption effects. The SICE algorithm can be considered as an update of the previous version of the algorithm (called S3Snow[6]) that appeared in the Snow Properties module of SNAP.

2.2 Validation

2.2.1 Snow spectral albedo

The validation of spectral albedo for the case of clean snow has been reported in [6], where a detailed description of the ground and satellite measurements, not repeated here, may be found. In the case of polluted snow, we follow a different procedure than that suggested in [6]. Here, we use the improved atmospheric correction, which explicitly accounts for molecular/aerosol light scattering and absorption effects. The results for the French Alps, Col du Lautaret validation site (45.041288N, 6.410557E, 2100 m a.s.l) on April 17, 2018 (Fig.1a) confirm that the current SICE planar albedo retrieval has a higher accuracy as compared to the earlier S3Snow algorithm [6] for the cases studied. Also unlike the S3Snow retrievals, there is a possibility to vary aerosol load in the framework of the updated retrieval, which is currently not the case for S3Snow plane albedo retrieval results. As it follows from Fig.1b, the variation of AOT (500nm) in the range 0.07-0.35 does not change the plane albedo retrieval accuracy (above 3% for the case studied). Note that the AOT(500nm) obtained from the Copernicus Atmospheric Monitoring Service near-real-time forecast product (https://www.ecmwf.int/en/about/what-we-do/environmental-services/copernicus-atmosphere-monitoring-service) was 0.125 for the case studied. We conclude that the precise information on the spectral aerosol optical thickness is not needed for the accurate snow spectral albedo retrievals for the low aerosol load characteristic for the Col du Lautaret validation site located at 2100m a.s.l. [4]. It should be pointed out that the discrepancy of satellite and ground plane albedo measurements is not solely due to the retrieval but also partially due to surface spatial inhomogeneity (local scale effects vs much broader scale satellite pixel effects), time difference between satellite and ground measurements, and influence of 3-D effects from surrounding mountains.

 doi:10.20944/preprints201911.0391.v1

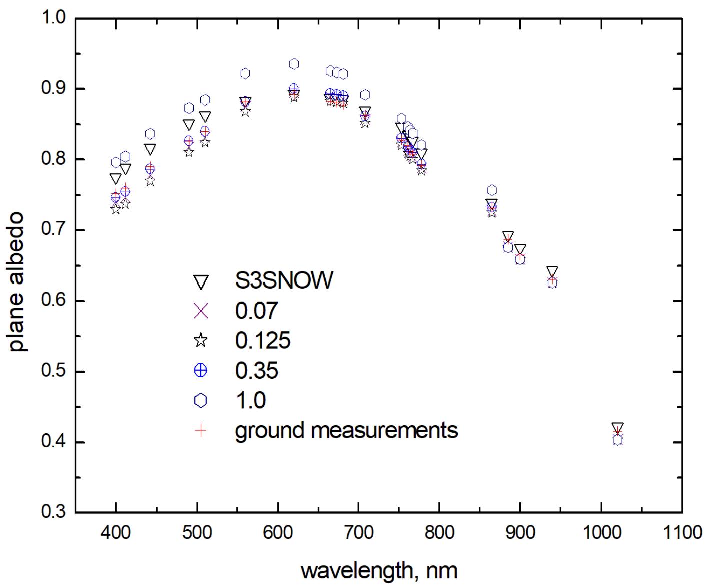

Fig.1a The plane albedo of dust laden snow retrieved from satellite measurements and measured on ground on April 17, 2018 at the at the Col du Lautaret validation site in the French Alps. In the retrieval process, four values of aerosol optical thickness (AOT) at 500nm were applied (0.07, 0.125, 0.35, and 1.0). The retrievals using S3Snow are also shown.

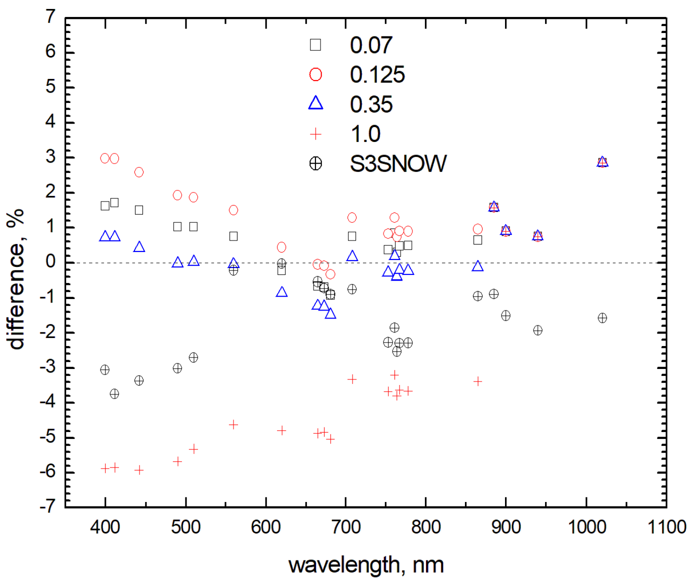

Fig.1b The differences in spectral plane albedo of dust laden snow retrieved from satellite measurements and measured on ground on April 17, 2018 at the at the Col du Lautaret validation site in the French Alps. In the retrieval process, four values of aerosol optical thickness (AOT) at 500nm in the framework of SICE have been assumed (0.07, 0.125, 0.35, and 1.0). The differences of satellite retrievals and ground measurements of plane albedo using S3Snow are also presented.

Preprints (www.preprints.org) | NOT PEER-REVIEWED | Posted: 30 November 2019 doi:10.20944/preprints201911.0391.v1

2.2.2 Snow broadband albedo

We validate broadband albedo (BBA) measured in the 0.3-2.4 micron wavelength range using ground measurements from fifteen Programme for the Monitoring Greenland Ice Sheet (PROMICE) automatic weather stations described further in [6]. The closest hourly observations are considered producing occasional more than one comparison each day for northern sites. A total of 4146 individual comparisons are made here. The PROMICE BBA data include a correction for measurement platform obstruction of the radiometer field of view [14] that increases average PROMICE BBA by 0.034. Clear sky conditions are estimated from downward longwave irradiance data [6].

At the PROMICE SCO_U location (Figs. 2-3, Table 3) on the eastern ice sheet, where clear sky conditions are common, we observe in three May – September years (2017, 2018, 2019) over a wide (0.52) BBA range (from 0.85 indicative of dry snow cover and 0.33 when snow cover has completely ablated to expose impurity rich bare ice) a very similar temporal pattern in the ground observations and from the OLCI retrievals.

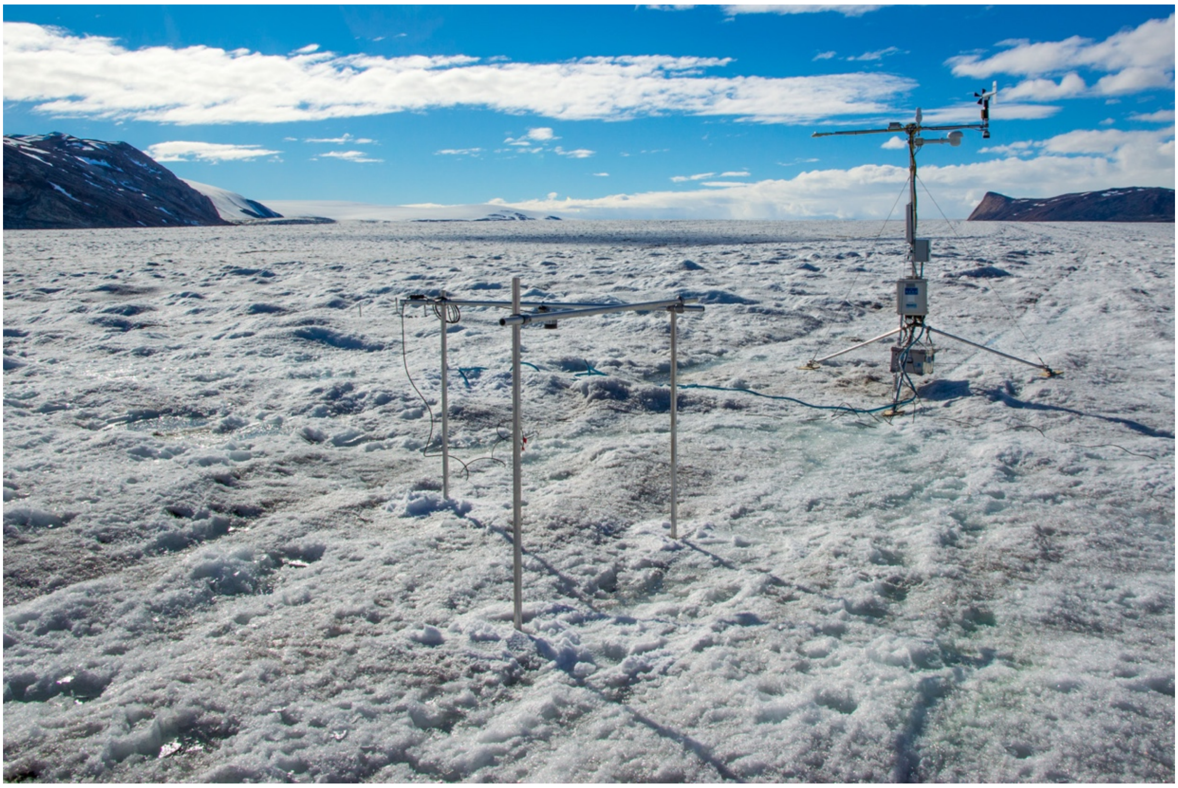

Fig. 2. The SCO_U PROMICE automatic weather station with radiometer on main station in background. The photo is from 4 August, 2017 under typical late-ablation season surface conditions with a surface comprised of mineral dust and biologically polluted bare ice as opposed to brighter seasonal snow cover.

 doi:10.20944/preprints201911.0391.v1

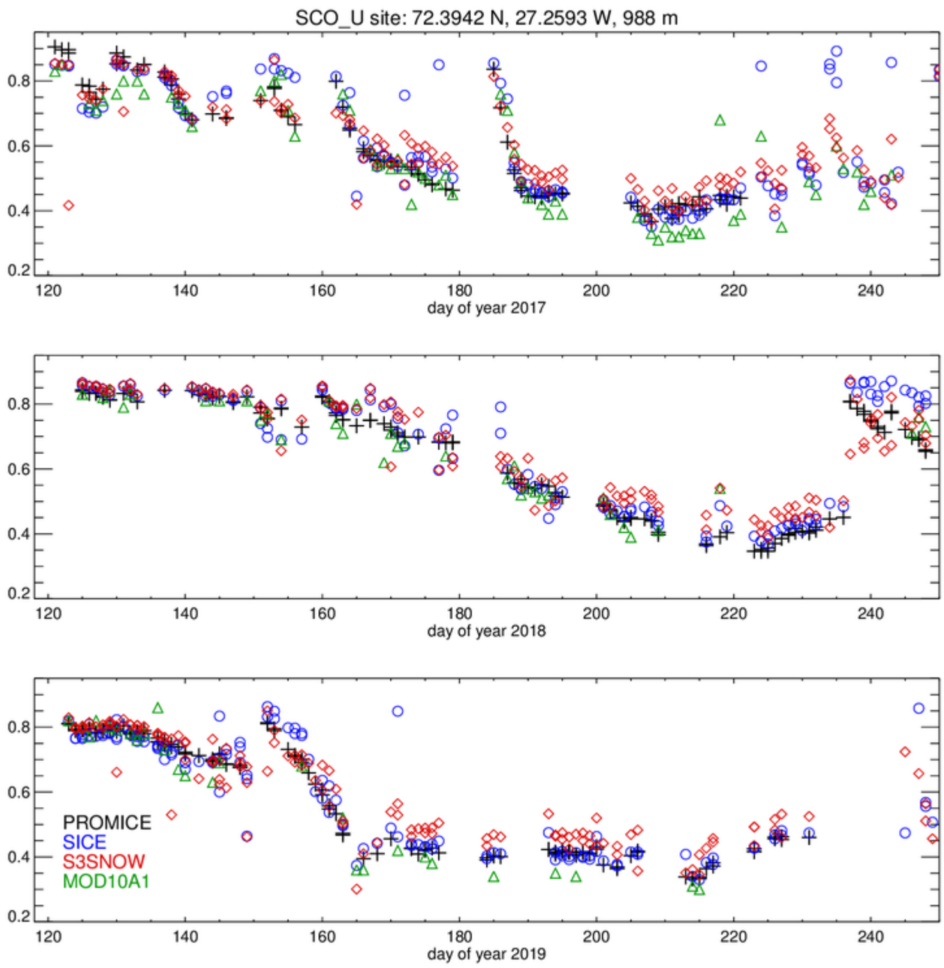

Fig.3. Example of the broadband albedo (BBA) time series from the SCO_U PROMICE automatic weather station site (Table 3) in comparison to the BBA retrievals from the current retrieval (SICE), the earlier OLCI retrieval after [6] (S3SNOW) and for the NASA MODIS MOD10A1 product [15].

Among the fifteen PROMICE locations, spanning a wide spatial scale (2076 km north-south (18.9° latitude) and 2390 m in elevation), SICE BBA agreement is as high as is realistic to expect with unattended observatio ns spanning three years (Table 3). We find regression slopes averaging insignificantly from unity, an average correlation coefficient of 0.861 and an average root-mean-square difference (RMSD) of 0.072. The average bias (-0.045) being higher than one standard deviation (0.029) suggests the measurement frame correction (+0.034) may be counter - productive. Clearly, the results with low correlation coefficients (see, e.g., EGP site in Table 3) not always mean bad retrievals. This is especially the case, when the BBA variability at the site (e.g., at the PROMICE EGP site) is low. We point out that the average bias at the EGP site located at 2660m above sea level is equal to the average (-0.045) although the correlation coefficient is just 0.659. If we do not account for the PROMICE station frame correction, the bias is just -0.011 for this site, which is an excellent retrieval result. One may expect that the PROMICE station frame correction may depend on the site location and time of year. This variability is not accounted for in our validation scheme.

The current approach, advanced from that reported in [6] by the improved atmospheric correction, has increased agreement with the PROMICE data, and an apparent accuracy that also exceeds that in the comparison with the NASA MODIS MOD10A1 albedo product (Figs. 4 – 5). Examples are made for the southern Greenland ice sheet QAS_L PROMICE location and the northwestern ice sheet THU_L PROMICE location (Fig. 4, right).

 doi:10.20944/preprints201911.0391.v1

Table 3. Validation statistics for broadband albedo at fifteen PROMICE Greenland ice sheet ground stations. Here, N is the number of closest hourly observations.

PROMICE station name	latitude, degrees north	longitude, degrees	elevation, m above sea level	regression slope	regression constant	correlation coefficient	mean SICE BBA-PROMICE BBA	RMSD	N
KPC_L	79.908	-24.080	366	0.828	0.147	0.958	-0.044	0.073	447
KPC_U	79.833	-25.163	865	0.768	0.191	0.800	-0.009	0.043	431
SCO_L	72.223	-26.818	459	1.071	0.000	0.958	-0.035	0.063	268
SCO_U	72.394	-27.259	988	1.061	0.011	0.971	-0.046	0.063	349
QAS_L	61.031	-46.849	270	1.017	0.017	0.972	-0.024	0.054	126
QAS_U	61.099	-46.833	621	0.987	0.143	0.865	-0.136	0.157	153
QAS_M	61.175	-46.820	892	0.842	0.130	0.961	-0.039	0.071	122
NUK_L	64.482	-49.538	527	0.584	0.190	0.743	-0.056	0.073	196
NUK_U	64.510	-49.271	1119	0.883	0.093	0.750	-0.016	0.103	192
KAN_L	67.095	-49.953	664	1.000	0.026	0.863	-0.026	0.038	194
KAN_U	67.000	-47.027	1842	0.462	0.455	0.686	-0.031	0.042	177
UPE_L	72.893	-54.295	211	1.465	-0.223	0.884	-0.044	0.089	241
UPE_U	72.887	-53.585	929	1.149	-0.021	0.886	-0.075	0.100	264
THU_L	76.400	-68.266	566	1.073	0.006	0.970	-0.051	0.069	346
THU_U	76.420	-68.146	761	1.053	-0.003	0.846	-0.035	0.066	329
EGP	75.625	-35.973	2660	0.591	0.369	0.659	-0.045	0.046	320
		average	**859**	**0.927**	**0.096**	**0.861**	**-0.045**	**0.072**	**260**
		st.dev.	**620**	**0.248**	**0.161**	**0.106**	**0.029**	**0.030**	**102**

Preprints (www.preprints.org) | NOT PEER-REVIEWED | Posted: 30 November 2019 doi:10.20944/preprints201911.0391.v1

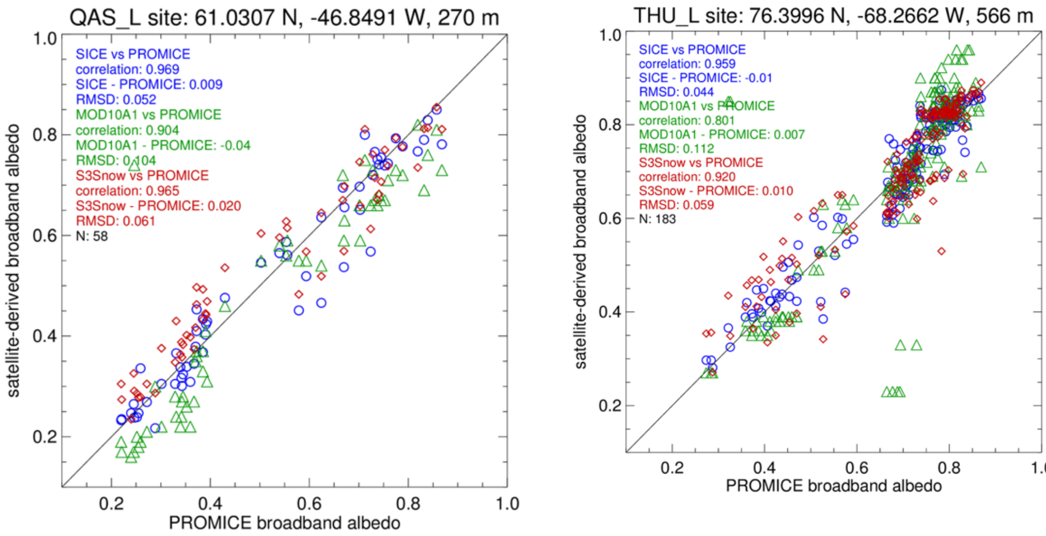

Fig.4. Examples of satellite derived and ground observations of snow and bare ice albedo. The left figure includes both the S3 Snow and the current processing results for the site QAS_L. The comparison uses cases only when all retrievals are available, i.e. including those from MODIS MOD10A1. The right figure is the same except for the site THU_L.

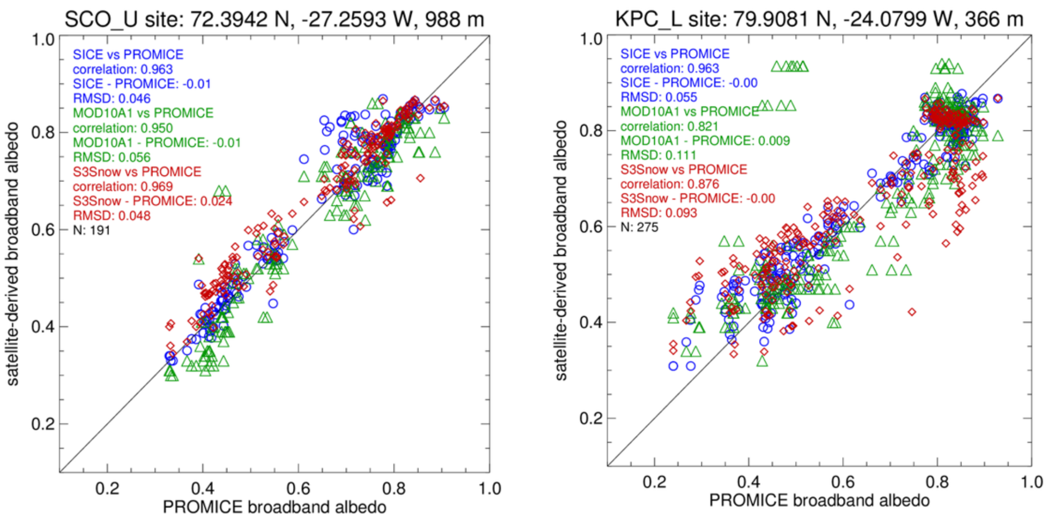

Fig.5. Same as Fig. 4 but for the SCO_U location (also illustrated in Fig. 3) (left) and for a northeastern location (KPC_L).

3. Discussion

Standard underlying surface albedo retrieval algorithms based on single view observations can be corrected for surface anisotropy effects using multiple day observations of reflected solar light for a given site to cover necessary illumination/ observation geometries needed for the respective integration procedures with respect to the corresponding zenith, viewing and relative azimuth angles. In our approach, we use the analytical relationship between the top-of-atmosphere reflectance and spherical albedo for clean snow underlying surface (Eqs. (1), (2)) in the near infrared (865 and 1020 nm), where atmospheric contribution to the signal as registered on a satellite is small, to derive

 doi:10.20944/preprints201911.0391.v1

the snow spherical albedo from measurements at a fixed illumination/observation geometry. Therefore, multiple day observations for the same site are not required and the snow albedo for a given place can be derived in one hour or so after the satellite acquisition time. In the case of polluted snow the spherical albedo is found from Eq.(9) for an assumed aerosol model. The technique also incorporates the calculation of plane spectral and broadband albedo. We have found that the errors of the Case 1 snow are usually in the range 1-2% in the visible as compared to the ground measurements [6]. They can increase to 3-5% for the spectral albedo in the near IR and also for polluted snow.

Water exists in three thermodynamic phases (liquid, sloid, gas) both in atmosphere and underlying surface. The separation of clean (Case 1) and polluted (Case 2) waters has been useful in oceanic remote sensing using spaceborne observations. We show that a similar separation of satellite retrievals for clean and polluted snow areas (Case 1 and Case 2 snow) useful in remote sensing of snow from space. Actually, a similar separation of cases is of importance in cloud remote sensing, where modern cloud remote sensing algorithms are based on the assumption of clean (Case 1) clouds. The polluted (Case 2) clouds exist but up to now their study is much less advanced.

In this paper we propose fast snow albedo retrieval techniques both for Case 1 and Case 2 snow. The results for the clean snow are more accurate and robust. The retrievals for the Case 2 snow are less accurate and are based on the simplified atmospheric correction procedure specified in Eq. (9) and general relationship between reflectance and albedo given by Eq. (10). We have found that influence of the aerosol load on the retrieval of the snow surface albedo is weak in the case of small atmospheric aerosol optical thickness characteristic for Arctic and alpine areas . As a matter of fact, Eq. (10) performs well not only for snow but also for other types of weakly absorbing and strongly scattering media such as clean and polluted bare ice. Therefore, the technique proposed here can be used to study also the albedo of terrestrial bare ice surfaces as demonstrated in Fig. 3-5, where low albedo values correspond actually not to snow but ice underlying surfaces.

4. Conclusions

Through comparison with independent ground observations, the proposed fast atmospheric correction technique is shown to perform accurately in a range of conditions from a 2100 m elevation mid-latitude location in the French Alps to a Greenland ice sheet network of 15 locations spanning a 2076 km north-south, 18.9 degrees latitude and 2390 m in elevation. It should be pointed out that snow albedo satellite retrievals are often biased due to the *assumed* shapes of ice grains (spheres, columns, fractal particles, etc.) used in the retrieval process. We have used the notion of the effective absorption length in this work. It makes it possible to include all shape-dependent constants in the value of EAL determined form the satellite measurements themselves. This reduces the snow grain shape effect on the retrievals (at least in the OLCI spectral range). The atmospheric correction is performed assuming the aerosol model and aerosol optical thickness ahead of retrievals. The associated errors do not lead to considerable errors in the retrieved snow albedo in case of low aerosol load as demonstrated in Fig.1.

The current approach, advanced from that reported in [6] by the improved atmospheric correction, has increased agreement with ground observations, and an apparent accuracy that also exceeds that of the NASA MODIS MOD10A1 broadband albedo product.

A next step is to process the full OLCI catalogue from Sentinel-3A and B satellites over 100% snow or ice covered areas of our planet using this new algorithm. The product would offer the climate research community a new enhanced quality snow and ice albedo product, which will lead to the advancement of our knowledge of snow albedo effects on the terrestrial climate change [1, 2].

 doi:10.20944/preprints201911.0391.v1

Author Contributions: Conceptualization, A.K., J. B.; methodology, J. B., A. K., A. S.; software, A. K., J. B., K. M.; validation, B. V., A. K., J. B., M. L.; formal analysis, A. K., A. S., J. B.; resources, J. B; data curation, J. B., K. M., B. V.; writing—original draft preparation, A. K., J. B.; writing—review and editing, A. K., J. B., M. L., B. V., A. S.; visualization, A.K., J. B., supervision, M. K., J. B.; project administration, M. K., J. B.; funding acquisition, J. B., A. K.

Acknowledgments: Agency (ESA) studies; the Scientific Exploitation of Operational Missions (SEOM) Sentinel-3 Snow (Sentinel-3 for Science, Land Study 1: Snow), ESRIN contract 4000118926/16/I-NB and the ESRIN contract 4000125043 - ESA/AO/1-9101/17/I-NB EO SCIENCE FOR SOCIETY. Additional support came from The Program for the Monitoring of the Greenland Ice Sheet (PROMICE), part of the Danish Energy Agency through the DANCEA program. The authors thanks M. Dumont and G. Picard for providing snow spectral albedo data used in this work for validation purposes and also V. Rozanov for providing data given in Table A1. The authors are grateful to the AERONET staff, PIs and site managers.

Conflicts of Interest: The authors declare no conflict of interest.

Appendix. Atmospheric radiative transfer: simple approximations

The top of atmosphere reflectance R_a for a clear atmosphere can be presented in the following way using the Sobolev approximation[16]:

$$R_a = R_{ss} + R_{ms}, \tag{A.1}$$

where single scattering contribution

$$R_{ss} = M(\tau)p(\theta) \tag{A.2}$$

and multiple light scattering contribution is approximated as

$$R_{ms} = 1 + M(\tau)q(\mu_0,\mu) - \frac{N(\tau)}{4+3(1-g)\tau}, \tag{A.3}$$

where

$$M(\tau) = \frac{1-e^{-m\tau}}{4(\mu_0+\mu)},\ N(\tau) = f(\mu_0)f(\mu), \tag{A.4}$$

$$f(\mu) = 1 + \frac{3}{2}\mu + \left(1 - \frac{3}{2}\mu\right)e^{-\frac{\tau}{\mu}}, m = \mu_0^{-1} + \mu^{-1}, \tag{A.5}$$

$$q(\mu_0,\mu) = 3(1+g)\mu_0\mu - 2(\mu_0+\mu). \tag{A.6}$$

Here, μ_0 is the cosine of the solar zenith angle (SZA), μ is the cosine of the viewing zenith angle (VZA) , θ is the scattering angle defined as

$$\cos\theta = -\mu_0\mu + s_0 s\cos\varphi, \tag{A.7}$$

φ is the relative azimuthal angle (equal to 180 degrees minus OLCI relative azimuthal angle), s_0 is the sine of the SZA, s is the sine of the VZA, τ is the atmospheric optical thickness, $p(\theta)$ is the phase function, g is the asymmetry parameter. It is determined by the following expression:

$$g = \frac{1}{2}\int_0^{\pi} p(\theta)\sin\theta\cos\theta\, d\theta. \tag{A.8}$$

The approximate account for aerosol absorption effects is performed multiplying R_{ss} (see Eq. (A2) by the single scattering albedo ω_0[17]. The accuracy of Eqs. (A1)-(A3) can be further improved using the truncation approximation as discussed in [16].

The transmission function $T(\mu_0,\mu)$ is approximated as follows:

$$T(\mu_0,\mu) = t^m, \tag{A.9}$$

where t is calculated using the following approximation[16]:

$$t = e^{-B\tau}. \tag{A.10}$$

Here,

$$B = \frac{1}{2}\int_{\frac{\pi}{2}}^{\pi} p(\theta)\sin\theta\cos\theta\, d\theta \tag{A.11}$$

is the so – called backscattering fraction. The atmospheric spherical albedo r_a is found using the approximation proposed in [11]:

$$r_a = \left(Me^{-\frac{\tau}{\varsigma}} + Ne^{-\frac{\tau}{\kappa}} + D\right)\tau. \tag{A.12}$$

The coefficients of polynomial expansions of all coefficients (M, N, D ,ς, κ) in Eq.(A.12) with respect to the value of g are given in [11].

One can see that the reflection function depends on the atmospheric optical thickness, which can be presented in the following form:

$$\tau(\lambda) = \tau_{mol}(\lambda) + \tau_{aer}(\lambda). \quad \text{(A.13)}$$

The molecular optical thickness can be approximated as [18,19]:

$$\tau_m(\lambda) = q\lambda^{-\upsilon}, \quad \text{(A.14)}$$

at the normal pressure p_0 and temperature t_0 . Here, $q = 0.008735$, $\upsilon = 4.08$, and the wavelength is in microns. We derive the value of molecular optical thickness at another pressure level p using the following expression: $\tau_{mol}(\lambda) = \hat{p}\tau_m(\lambda)$, where $\hat{p} = \frac{p}{p_0}$, p is the site pressure, $p_0 = 1013.25mb$. The site pressure is calculated using the following equation: $p = p_0 \exp\left(-\frac{z}{H}\right)$. Here z is the height of the underlying surface provided in OLCI files and *H=7.64km* is the scale height.

It follows for the aerosol optical thickness (AOT)[4]:

$$\tau_{aer}(\lambda) = \beta\left(\frac{\lambda}{\lambda_0}\right)^{-\alpha}, \quad \text{(A.15)}$$

where $\lambda_0 = 0.5\mu m$, the pair (α, β) represents the Angström parameters. We did not make an attempt to derive the pair (α, β) over snow. These values must be assumed ahead of retrievals (e.g., using aerosol climatology [20], ground measuremnets or aerosol forecasts) . The statistical results for the values α, β over various Greenland AERONET [21] stations are given in Figs. A1, A2. It follows that over Greenland the value of $\beta = \tau_{aer}(\lambda_0)$ is in the range 0.02-0.12 on average (see Fig.A1). For our BBA albedo retrievals reported in this paper we assume that $\beta = 0.07$ independently on location and time. The AERONET monthly statistics shows that α is in the the range 1.0-1.6 over Greenland (see Fig. A2). Therefore, we assume the value of $\alpha = 1.3$ in our retrievals.

The phase function can be presented in the following form:

$$p(\theta) = \frac{\tau_{mol}p_{mol}(\theta) + \tau_{aer}p_{aer}(\theta)}{\tau_{mol} + \tau_{aer}}, \quad \text{(A.16)}$$

where

$$p_{mol}(\theta) = \frac{3}{4}(1 + \cos^2\theta) \quad \text{(A.17)}$$

is the molecular scattering phase function and $p_{aer}(\theta)$ is the aerosol phase function. We shall represent this function as:

$$p_{aer} = \frac{1 - g_{aer}^2}{(1 - 2g_{aer}\cos\theta + g_{aer}^2)^{\frac{3}{2}}}. \quad \text{(A.18)}$$

Therefore, it follows for the asymmetry parameter:

$$g = \frac{\tau_{aer}}{\tau_{mol} + \tau_{aer}} g_{aer}. \quad \text{(A.19)}$$

The parameter g_{aer} varies with the location, time, aerosol, type, etc. We shall assume that it can be approximated by the following equation:

$$g_{aer} = g_0 + g_1 e^{-\frac{\lambda}{\lambda_0}}. \quad \text{(A.20)}$$

The coefficients in this equation (as derived from multiple year AERONET observations over Greenland, see Fig.A3) are as follows:

$$g_0 = 0.5263, g_1 = 0.4627, \lambda_0 = 0.4685\mu m. \quad \text{(A.21)}$$

The parameter B for the Henyey-Greenstein can be represented via the complete elliptic integral of the first kind K(g) as follows [24]:

$$B(g) = \frac{1-g}{2s(g)}, \quad \text{(A.22)}$$

where

$$s(g) = \frac{g}{2(1+g)K(g)/\pi - 1}, \quad \text{(A.23)}$$

$$K(g) = \int_0^{\pi/2} \frac{dv}{\sqrt{1 + g^2 \sin^2 v}}, \quad \text{(A.24)}$$

It follows from Eq. (A.24) that *K(0)=π/2* and, therefore, *s(0)=1, B(0)=1/2* as it should be for isotropic (and Rayleigh) scattering. The function *s(g)* can be approximated by the following analytical expression:

$$s(g) = \upsilon + \frac{\varsigma}{1 + \exp((g - \zeta)/\kappa)}, \quad \text{(A.25)}$$

Preprints (www.preprints.org) | NOT PEER-REVIEWED | Posted: 30 November 2019 doi:10.20944/preprints201911.0391.v1

where $\upsilon = -6.7012$, $\varsigma = 7.8049$, ζ =2.1978, $\kappa = 0.51656$. The accuracy of Eq. (A.25) is better than 1.5% at g≤ 0.9.

It should be pointed that the system of equations given above enables the callculation of underlying snow-atmosphere reflectance as a function of the aerosol optical thickness for a known value of the snow spherical albedo (see Eq. (9)).

As far as gaseous transmission is of concern, we propose to use the following exponential approximation [25]:

$$T_{ozone} = \exp(-m\gamma\tau_{ozone}), \qquad (A.23)$$

where

$$\gamma \;\; = \frac{c_{O3}}{c}. \qquad (A.24)$$

Here, c_{O3} is the ozone concentration provided in the OLCI satellite file (with account for units) and τ_{ozone} is the vertical optical depth of ozone at the concentration $c = 405\text{DU}$. In particular, to transfer from OLCI O3 units (kg/ m^2) to Dobson Units (DU), we multiply OLCI O3 concentration by a constant factor equal to 4.6729e+4. Therefore, the total ozone load 300DU corresponds to 6.42e-3 kg/ m^2. The values τ_{ozone} calculated for all OLCI channels at c=405 DU with account for the instrument response function are given in Table A1.

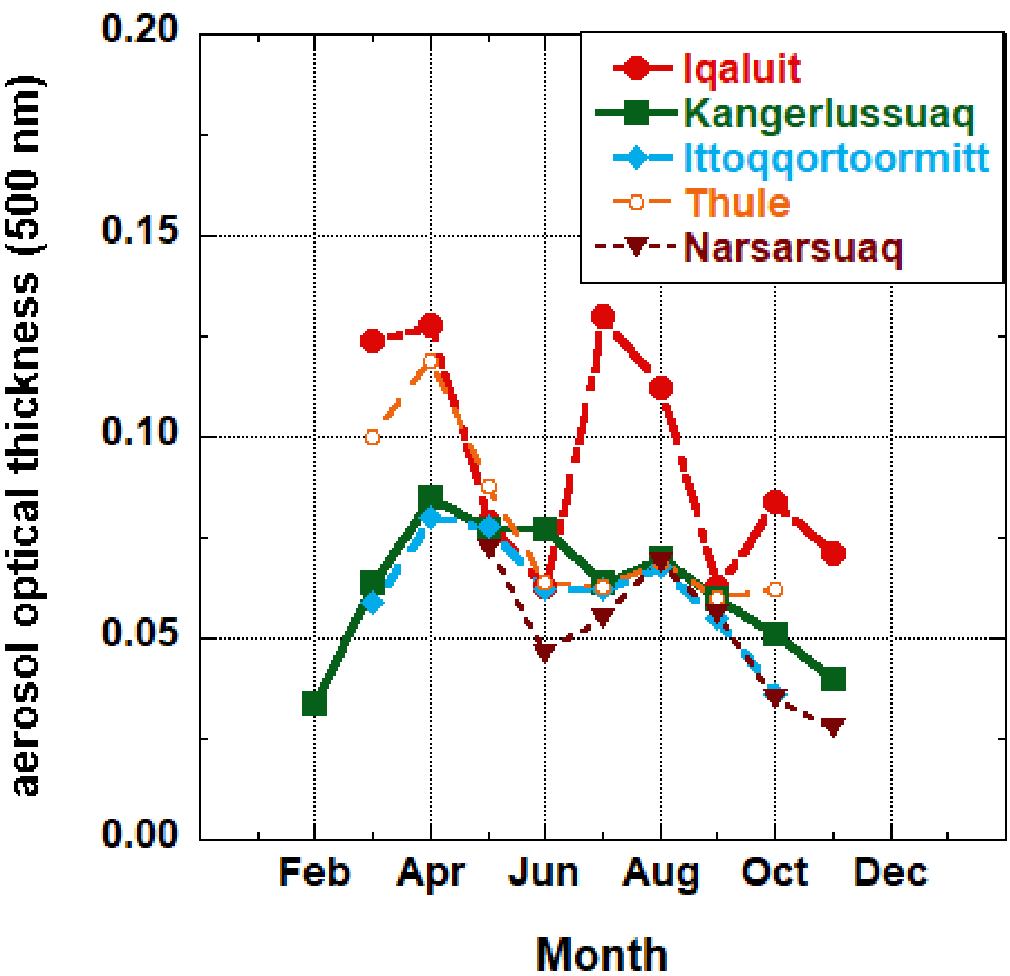

Fig. A1. The statistical properties of the aerosol optical thickness at 500nm over various AERONET stations in Greenland. The results are derived from Level 2 (Verison 3 [22]AERONET data) for years 2007-2017.

doi:10.20944/preprints201911.0391.v1

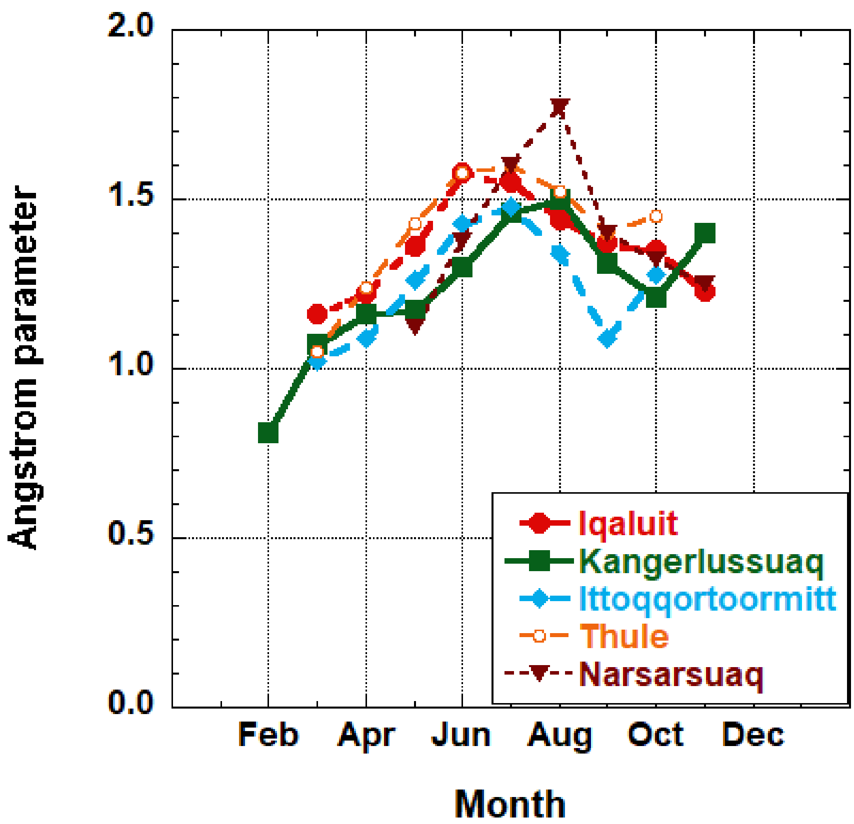

Fig. A2. The statistical properties of the Angstroem parameter for atmospheric aerosol over various AERONET stations in Greenland. The results are derived from Level 2 (Verison 3 [22]AERONET data) for years 2007-2017.

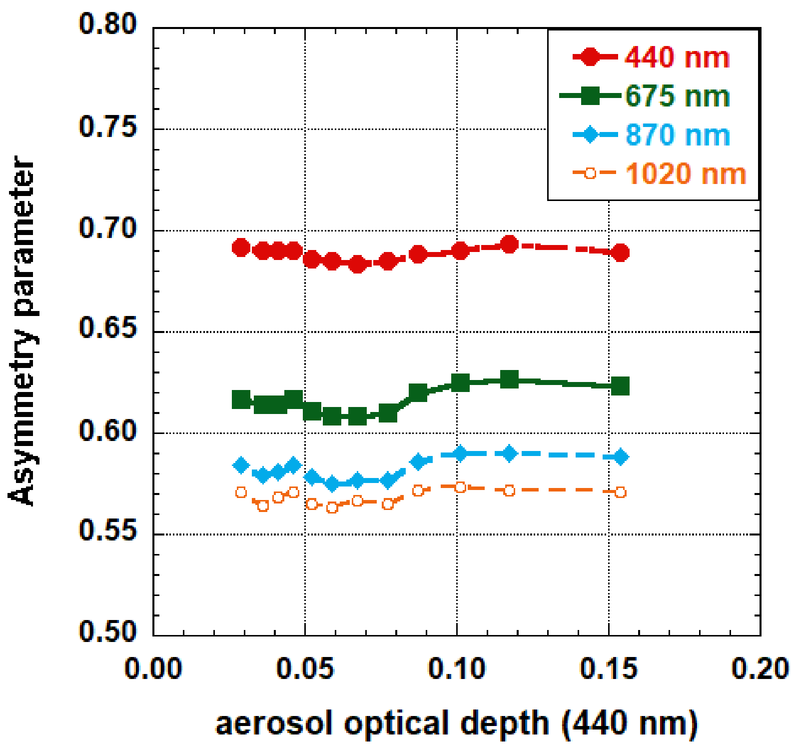

Figure A3. The asymmetry parameter climatology (2007-2017) for five considered sites in Greenland (version 3 [23]) data, Level 1.5 retrievals with the residual error <5%, and AOT (440 nm) <0.20). Total number of retrievals is 5316 divided in 12 groups with 443 asymmetry parameters in each group.

Preprints (www.preprints.org) | NOT PEER-REVIEWED | Posted: 30 November 2019 doi:10.20944/preprints201911.0391.v1

Table A1. The spectral dependence of ozone vertical optical thickness τ_{ozone} in terrestrial atmosphere at the ozone load equal to 405 DU. The results are derived assuming particular shapes of temperature, pressure, and ozone concentration vertical distribution as discussed in [25]. We have found that the variation of profiles does not change the value of τ_{ozone} significantly.

λ, nm	τ_{ozone}
400.00000	1.378170469E-004
412.50000	3.048780958E-004
442.50000	1.645714060E-003
490.00000	8.935947110E-003
510.00000	1.750535146E-002
560.00000	4.347104369E-002
620.00000	4.487130794E-002
665.00000	2.101591797E-002
673.75000	1.716230955E-002
681.25000	1.466298300E-002
708.75000	7.983028470E-003
753.75000	3.879744653E-003
761.25000	2.923775641E-003
764.37500	2.792211429E-003
767.50000	2.729651478E-003
778.75000	3.255969698E-003
865.00000	8.956858078E-004
885.00000	5.188799343E-004
900.00000	6.715773241E-004
940.00000	3.127781417E-004
1020.00000	1.408798425E-005

 doi:10.20944/preprints201911.0391.v1

References

[1] Vinnikov, K. Y.; Robock, A., Stouffer, R.J., et al. Global warming and Northern Hemisphere sea ice extent. *Science* **1999**, 286, 1934-1937.

[2] Hansen, J.; Nazarenko, L. Soot climate forcing via snow and ice albedos. *Proc. Natl. Acad. Sci.* **2004**, 101, 423-428, doi:10.1073/pnas.2237157100.

[3] Stroeve, J.; Box, J. E.; Wang, Z., Schaaf, C., Barrett, A. 2013: Re-evaluation of MODIS MCD43 Greenland albedo accuracy and trends. *Remote Sensing of Environment* **2013**,138, 199-214.

[4] Kokhanovsky and Tomasi, eds. *Physics and Chemistry of Arctic atmosphere*, **2020**. Berlin: Springer, in press.

[5] Schaaf, C. B.; Gao, F.; Strahler, A.H., et al. First operational BRDF, albedo and nadir reflectance products from MODIS. *Remote Sens. Env.* **2002**, 83, 135-148.

[6] Kokhanovsky, A. A.; et al. Retrieval of Snow Properties from the Sentinel-3 Ocean and Land Colour Instrument. *Remote Sensing* **2019** *11*(19), 2280; https://doi.org/10.3390/rs11192280.

[7] Dang, C.; Brandt, R. E.; Warren, S. G. Parameterizations for narrowband and broadband albedo of pure snow, and snow containing mineral dust and black carbon. *J. Geophys. Res*. **2015**, 120, doi:10.1002/2014JD022646.

[8] Morel, A.; Prieur, L. Analysis of variations in ocean color. *Limnol. Oceanogr*., **1977**, 22, 709-722.

[9] Mobley, C.D.; Stramski, D., Bissett, W.P.; Boss, E. Optical modeling of ocean waters: Is the Case 1 - Case 2 classification still useful? *Oceanography* **2004**, 60-67.

[10] Liou, K.-N. *An introduction to Atmospheric Radiation* **2002**, N. Y.: Academic Press.

[11]Kokhanovsky, A.; Mayer, B.; Rozanov, V.V. A parameterization of the diffuse transmittance and reflectance for aerosol remote sensing problems. *Atmospheric Research* **2005**, 73, 37-43.

[12] Ricchiazzi, P. ; Yang, S. ; Gautier, C. ; Sowle, D. SBDART, A research and teaching tool for plane-parellel radiative transfer in the Earth's atmosphere, *Bul. Am. Meteorol. Soc.* **1998**, 79, 2101–2114.

[13] Shettle, E. P.; Fenn, R. W. Models for the aerosols of the lower atmosphere and the effects of humidity variations on their properties. Report AFGt-TR-79-O21 **1979**, Air Force Geophysical Laboratory, USA.

[14] Aoki, T.; Kuchiki, K.; Niwano, M.; Kodama, Y.; Hosaka, M.; Tanaka, T. Physically based snow albedo model for calculating broadband albedos and the solar heating profile in snowpack for general circulation models. *J. Geophys. Res. Atmos.* 2011, 116.

[15] Hall, D.K. & Riggs, G.A. 2016: MODIS/Terra Snow Cover Daily L3 Global 500m Grid, Version 6. Greenland coverage. National Snow and Ice Data Center, NASA Distributed Active Archive Center, Boulder, Colorado USA. http://nsidc.org/data/MOD10A1/versions/6, accessed December 2016.

[16] Sobolev, V. V. *Light scattering in planetary atmospheres* , M.: Nauka, **1972**.

[17] Katsev, I. L.; Prikhach, A. S.; Zege, E. P.; Grudo, J. O.; Kokhanovsky, A. A.: Speeding up the aerosol optical thickness retrieval using analytical solutions of radiative transfer theory. *Atmos. Meas. Tech*. **2010**, 3, 1403–1422, https://doi.org/10.5194/amt-3-1403-2010.

[18] Leckner, B.The Spectral Distribution of Solar Radiation at the Earth's Surface-Elements of a Model. *Sol. Energy* **1978,** 20, 143-150.

[19] Iqbal, M. An Introduction to Solar Radiation **1983**, Academic Press: New York, pp. 114-115.

[20] Kinne, S. The MACv2 Aerosol Climatology. *Tellus B*, **2019**, 71, 1–21 (data: ftp://ftp-projects.zmaw.de/aerocom/climatology/MACv2_2018/).

[21] Holben, B.N.; et al., An emerging ground-based aerosol climatology: Aerosol optical depth from AERONET, *J. Geophys. Res*. **2001**, 106, 12,067-12,097.

[22] Giles, D.M.; et al. Advancements in the Aerosol Robotic Network (AERONET) Version 3 database – Automated near real-time quality control algorithm with improved cloud screening for Sun photometer aerosol optical depth (AOD) measurements, *Atmos. Meas. Tech*. **2019**, 12, 169-209, https://doi.org/10.5194/amt-12-169-2019.

[23] Sinyuk, A.; et al. The AERONET Version 3 aerosol retrieval algorithm, associated uncertainties and comparisons to Version 2. *Atmos. Meas. Techniques* **2020**, to be submitted.

[24] Wiscombe, W.J.; Grams, G. W. The backscattered fraction in two-stream approximations, *J. Atmos. Sciences* **1976**, 33, 2240-2451.

[25] Kokhanovsky, A.A.; et al., 2020: The retrieval of total ozone over snow using Ocean and Land Colour Instrument, J, Quantitative Spectroscopy and Radiative Transfer**2020**, in preparation.